This article has been accepted for publication in IEEE Transactions on Wireless Communications. This is the author's version which has not been fully edited and content may change prior to final publication. Citation information: DOI 10.1109/TWC.2025.3649587

RIS Assisted Smart Radio Environment for Enhanced Non-Orthogonal Multiplexing Indoor Positioning System

Somayeh Bazin, Keivan Navaie *Senior Member, IEEE*

***Abstract*—Indoor Positioning Systems (IPS) based on Received Signal Strength (RSS) often face challenges in achieving high accuracy due to spatial and temporal uncertainties in complex indoor environments. To address these limitations, this paper proposes a novel Static Reconfiguration Algorithm (SRA) leveraging Reconfigurable Intelligent Surface (RIS) technology to optimize RSS distributions. Unlike traditional methods, the SRA eliminates the need for dynamic RIS reconfiguration, instead employing a static approach that maximizes differentiation between RSS values at predefined Reference Points (RPs). This enhances localization precision by reducing spatial correlation and improving distinguishability, even in noisy environments. Simulation results demonstrate that the SRA significantly outperforms conventional RSS-based approaches, achieving positioning errors as low as 75 cm in high-noise scenarios compared to 150 cm with traditional methods. Furthermore, the algorithm proves effective across broader RSS measurement ranges (-100 to 0 dB) and achieves superior performance even with a single Access Point (AP). The multidimensional SRA approach further enhances accuracy by leveraging diverse RSS distributions through additional APs and time-division multiplexing. These results underscore the robustness, scalability, and efficiency of the SRA, positioning it as a transformative solution for next-generation IPS in smart environments.**

***Index Terms*—Indoor positioning systems, Re-configurable intelligent surface, Received signal strength.**

I. Introduction

Future wireless networks will deliver advanced, context-aware applications by integrating communication, sensing, and computing within the 6G platform. Central to this vision is precise user-location knowledge.

Accurate localization of users and IoT devices [1] underpins next-generation applications, driving demand for location-based services across smart cities [2], smart buildings [3], machine-type communication [4], IoT applications [5], healthcare, industry, and disaster management [6]–[8]

By addressing these requirements, future wireless networks will be poised to fully harness the potential of context-aware services, with Reconfigurable Intelligent Surfaces (RIS) emerging as a foundational technology for 6G [9]. RIS represents a paradigm shift in wireless communication, enabling dynamic control over the propagation environment to significantly improve signal quality, energy efficiency, and spatial awareness. These advanced capabilities pave the way for transformative solutions across a wide range of applications, including ultra-reliable low-latency communications (URLLC), enhanced mobile broadband (eMBB), and massive IoT connectivity. [10], [11]. While Global Positioning Systems (GPS) perform well outdoors, achieving accurate localization in indoor environment presents substantial challenges. Multipath effects, signal blockage, and complex indoor structures lead to unreliable performance with conventional methods like GPS.

S. Bazin and K. Navaie are with the School of Computing and Communications, Lancaster University, Lancaster, LA1 4WA, UK.

K. Navaie is also with the Alan Turing Institute, London, NW1 2DB, UK.

This work was submitted on xxxx, revised xxxx.

A. The State-of-the-Art and Its Limitations

Indoor Positioning Systems (IPS) address GPS limitations using metrics such as RSS [12], CSI [13], AoA [14], and TDoA [15]. Among these, RSS is widely adopted for its simplicity, scalability, and hardware efficiency, requiring neither precise synchronization nor antenna arrays. Typical RSS methods include multilateration and fingerprinting.

Multilateration relies on geometric principles, estimating the user's position based on distances inferred from RSS measurements [16]. Multilateration is conceptually simple but unreliable under None Line of Sight (NLoS) and multipath conditions, where variable attenuation distorts the distance–signal relation. Fingerprinting, on the other hand, maps pre-recorded RSS to locations using classifiers such as K-Nearest Neighbor (KNN), Artificial Neural Networks (ANN), offering practical deployment without additional hardware [17], [18].

1) The Role of Reconfigurable Intelligent Surfaces (RIS)

RIS has emerged as a transformative technology for overcoming the limitations of traditional IPS. RIS enables the dynamic control of signal propagation by configuring passive reflecting elements to alter signal paths [19]. This active manipulation introduces a new dimension to indoor positioning, allowing the customization of radio environments. Several studies have explored the application of RIS in enhancing IPS performance. Recent surveys, such as [20], have summarized key advances and challenges in RIS-assisted localization. In addition, distributed RIS architectures for indoor positioning have also been investigated, where multiple spatially separated surfaces jointly assist localization [21]

Separately, one study demonstrated how RIS can enhance the diversity of radio maps, achieving a significant 33% improvement in accuracy [22]. Another explored the integration of ultra-wideband (UWB) with RIS in a single Access Point (AP), further highlighting the potential of RIS to improve localization performance [23].

A different approach employed RIS to customize the RSS distribution, demonstrating its potential to significantly enhance localization accuracy [24]. For multi-user scenarios, the configuration of RIS was optimized based on the RSS values of individual users. However, this required the use of Time Division Multiplexing (TDM) to allocate separate time slots and configurations for each user, limiting the scalability of the solution.

2) Limitations of Current RIS Approaches

Despite the promising advancements enabled by RIS, significant challenges remain. One of the primary issues is the complexity of optimizing RIS configurations. Achieving optimal signal propagation requires determining a large number of coefficients, creating a vast search space that becomes increasingly difficult to navigate, particularly in dynamic environments where conditions change frequently.

In multi-user scenarios, simultaneous interactions between users introduce additional layers of complexity. Advanced coordination mechanisms are required to minimize interference and ensure accurate positioning, further complicating the optimization process. Additionally, relying on techniques such as TDM to allocate RIS configurations in multi-user scenarios raises concerns about scalability, as these methods can lead to delays or reduced responsiveness in real-time applications.

The current state of the art underscores the potential of RIS technology but also highlights the need for more efficient and scalable approaches. Optimizing RIS configurations to maximize the Euclidean distance between the RSS values of neighboring Reference Points (RPs) offers a promising direction. By reducing the likelihood of false positioning and enhancing overall accuracy, such approaches could unlock the full potential of RIS in next-generation IPS, bridging the gap between theoretical advancements and practical applications.

B. Proposed Solution and Key Results

This paper proposes a Static Reconfiguration Algorithm (SRA) for RIS that optimizes signal propagation to create a Maximum Differentiated RSS (MDRSS) distribution. SRA selects and tunes a subset of RIS elements to maximize RSS separation among RPs, enhancing accuracy and noise resilience. Through simulations, SRA demonstrated a broader RSS measurement range (-100 to 0 dB) compared to conventional methods (-72 to -70 dB), improving the distinguishability between neighbouring RPs. The algorithm outperformed conventional RSS fingerprinting approaches, achieving positioning errors as low as 75 cm in high-noise scenarios (standard deviation of 16), compared to 150 cm with traditional methods.

Notably, SRA delivered superior accuracy even with a single AP, outperforming multi-AP configurations in conventional systems. The multidimensional SRA approach further enhanced accuracy by leveraging diverse RSS distributions through additional APs and time-division multiplexing, effectively utilizing increased RSS dimensionality to handle noise and spatial correlation. Additionally, increasing the RSS measurement range significantly reduced false positioning, with a range of -100 to 0 dB providing greater differentiation between RPs than narrower ranges. These results highlight the robustness, scalability, and efficiency of SRA in achieving exceptional localization performance, making it a promising solution for modern indoor positioning challenges.

The SRA targets compact indoor environments such as offices or labs, delivering consistent sub-meter accuracy despite movement or obstacles—addressing the growing demand for fine-grained, robust localization [25].

It is important to emphasize that the accuracy improvement of the proposed SRA arise from ability to (i) reduce spatial correlation, (ii) expand RSS dynamic range, (iii) adapt to user movement with static optimization, and (iv) leverage multidimensional RSS for noise resilience. Although the RIS configuration remains static, its optimized surface parameters interact dynamically with environmental changes, providing both accuracy and efficiency compared with dynamic beam-steering schemes

The key contributions of this paper are as follows:

1) *Optimized RSS Distribution with MDRSS*: Building on the concept introduced in [24], the SRA algorithm generates an RSS distribution that maximizes differentiation between RPs. This enables accurate multi-user support without requiring dynamic RIS reconfiguration for each user. Instead, RIS reconfiguration is utilized to enhance localization accuracy by introducing diversity into the RSS distribution. Multi-user support is achieved by ensuring that each user benefits from the optimized SRA configuration, thereby minimizing localization errors without individualized RIS adjustments.
2) *Enhanced Localization Accuracy in Noisy Environments*: Simulation results demonstrate the superior performance of SRA in achieving high localization accuracy under various noise conditions. For instance, in environments with an RSS standard deviation of 16, the SRA achieves an average accuracy of approximately 75 cm, compared to 150 cm with conventional methods. Furthermore, in low-noise scenarios with a standard deviation of 2, the SRA achieves an accuracy of 40 cm, while conventional methods only reach 150 cm. This demonstrates the algorithm's robustness in both noisy and less noisy conditions.
3) *Intelligent RIS Element Selection*: The SRA incorporates an intelligent and computationally efficient approach to RIS element selection. The algorithm identifies the optimal active elements that maximize localization accuracy while keeping the number of required RIS elements low. This sparse-based selection minimizes computational complexity while maintaining reliability, making SRA faster and more efficient than state-of-the-art methods.
4) *Integration of Multipath Effects*: Unlike prior approaches (e.g., [22]–[24]), the SRA explicitly accounts for multipath impacts in indoor environments. This ensures the robustness of the algorithm in complex scenarios where multipath effects significantly influence signal propagation.

C. Gap Analysis

RIS have shown substantial promise in enhancing localization accuracy; however, many current solutions remain heavily dependent on extensive infrastructure and a large number of RIS elements. These dependencies introduce significant challenges for practical deployment. For example, [26] describes a fingerprint-based indoor localization system that requires repeated reconfiguration of the RIS to generate a RSS vector, illustrating the complexity of achieving accurate localization through iterative configurations. Similarly, [27] highlights the need for a large number of RIS elements to achieve high-resolution localization, demonstrating that precise positioning often incurs considerable infrastructure complexity.

While these approaches are effective in achieving high accuracy, they face critical scalability challenges. The requirement for numerous RIS elements and APs significantly increases deployment costs and limits the feasibility of large-scale implementations. Additionally, existing systems often struggle to adapt to dynamic environments. Research such as [28] and [29] identifies several environmental factors—including changes in user density, multipath effects, and variations in indoor conditions—as critical hurdles for IPS. These challenges underscore the need for solutions that combine high accuracy with adaptability and efficiency, without excessive infrastructure demands.

The proposed SRA method addresses these limitations by employing efficient resource allocation strategies. By intelligently selecting a subset of RIS elements, SRA reduces dependence on extensive infrastructure, achieving high localization accuracy with fewer RIS elements and APs. This optimization significantly enhances scalability and cost-effectiveness, making RIS-based localization systems more viable for real-world deployment. Moreover, SRA adapts to multi-user scenarios and environmental variations by leveraging a MDRSS distribution. Unlike conventional methods, SRA achieves robust performance without the need for additional computational resources or frequent adjustments to RIS configurations.

This adaptability ensures reliable operation in complex and evolving indoor environments, positioning SRA as a scalable, efficient, and resilient alternative to existing RIS-based localization approaches. The method's ability to balance accuracy, scalability, and adaptability makes it a compelling solution for advancing practical indoor localization systems.

Although this study emphasizes algorithmic and simulation analysis, real deployment would require RIS calibration and synchronization with existing Wi-Fi or Bluetooth infrastructure. SRA's static configuration can be pre-programmed on low-power hardware, enabling practical low-latency localization.

D. Structure of the Paper

The paper is structured as follows: Section II describes the system model. Section III formulates the RIS coefficient optimization problem. Section IV introduces the SRA, while Section V extends it to a multidimensional version. Section VI presents simulation results and comparisons. Conclusions are given in Section VII.

II. System Model

Fig. 1 presents a simplified schematic of an indoor environment where RIS panels are strategically deployed to enhance communication between a transmitter and a receiver. This model segments the area into multiple RPs, each uniquely labelled. Users within these areas receive signals from both the RIS panels and the AP. This configuration highlights the pivotal role of RIS in improving signal propagation and coverage in indoor environments.

A. RIS Assisted Signal Propagation Model

In general, the indoor channel impulse response is

$$h(t) = \sum_{k}^{K} \alpha_k e^{j\theta_k} \delta(t - \tau_k). \tag{1}$$

Here, α_k, θ_k, and τ_k represent the channel gain, uniformly distributed phase shift [30], and propagation delay of each individual path, respectively. The index k denotes the specific path among the total K paths, while δ refers to the Dirac delta function. in (1) α_k, θ_k, and τ_k are treated as time-invariant random variables. For an environment with I RPs, the received signal at ith RP is

$$y_{\mathrm{AP-RP_i}}(t) = \sum_{k} \alpha_{k,i} g(t - \tau_{k,i}) e^{j\left(\omega(t-\tau_{k,i})+\theta_{k,i}\right)}, \tag{2}$$

where ω denotes the angular frequency, and $g(t)$ represents the baseband pulse, modelled as a periodic square pulse with a width of W and a period of T, where $T > W$. Additionally, $\alpha_{k,i} = \frac{\lambda}{4\pi} \cdot \frac{\sqrt{G_t G_r}}{d}$ and $\tau_{k,i} = \frac{d}{C}$, where λ is the wavelength, d is the distance between the transmitter and receiver (with the receiver located at the ith RP), C is the speed of light, and G_t and G_r are the antenna gains of the transmitter and receiver, respectively. In addition to the aforementioned multipath links, RIS systems also account for the composite AP-RIS-RP links.

For an RIS comprising N reflector elements, each element receives the propagated signal from the AP and reflects it according to the following

$$y_{\mathrm{out,n}}(t) = \beta_n y_{\mathrm{in,n}}(t - t_n), \tag{3}$$

where β_n and t_n are adjustable amplitude and delay coefficients of the nth RIS element. Let $\mathbf{\Gamma} = [\Gamma_1, \Gamma_2, \ldots, \Gamma_N]$, where $\Gamma_n = [\beta_n, t_n]$, represents the vector of reflection coefficients of the RIS. Also $(\tau_n, \tau'_{n,i})$, $(\alpha_n, \alpha'_{n,i})$, and $(\phi_n, \phi'_{n,i})$ correspond to the delay, amplitude, and phase shift of the AP-RIS and RIS-RP links, respectively. The system operation is based on a narrowband RSS-based system with GHz carrier frequency, where the assumed bandwidth remains small relative to the carrier frequency.

For simplicity, we assume no signal coupling occurs between neighboring RIS elements, meaning each RIS element reflects incident signals independently. Additionally, we only consider signals that are reflected by the RIS for the first time, ignoring those that undergo multiple reflections. Therefore,

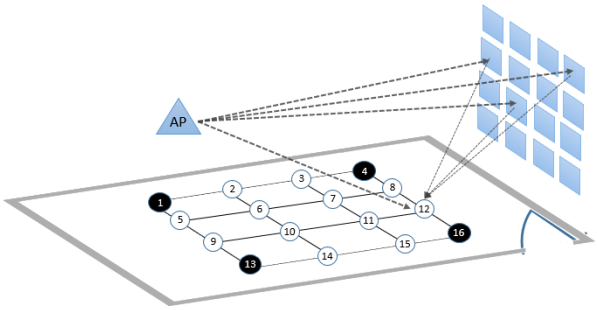

Fig. 1. Schematic representation of signal propagation in the system model, illustrating the segmentation of the area into distinct RPs. The center of each RP receives signals from both the AP and the RIS elements.

received signal from all RIS elements can be modeled as the superposition of their individually reflected signals:

$$y_{\text{AP}-\text{RIS}_n-\text{RP}_i}(t) = \sum_{n}^{N} \beta_n \alpha_n \alpha'_{n,i} g(t - t_n - \tau_n - \tau'_{n,i}) .e^{j\left(\omega(t-t_n-\tau_n-\tau'_{n,i})+\phi_n+\phi'_{n,i}\right)}. \quad (4)$$

We then set

$$B_{n,i} = \beta_n \alpha_n \alpha'_{n,i}, \mu_{n,i} = t_n + \tau_n + \tau'_{n,i}, \theta_{n,i} = \phi_n + \phi'_{n,i}. \quad (5)$$

Hence

$$y_{\text{AP}-\text{RIS}_n-\text{RP}_i}(t) = \sum_{n}^{N} B_{n,i} g(t - \mu_{n,i}) e^{j\left(\omega(t-\mu_{n,i})+\theta_{n,i}\right)}. \quad (6)$$

The received signal at each RP consists of Line-of-Sight (LoS) and None-Line-of-Sight (NLoS) components of AP-RP multipath channels and N reflected signal from AP-IRS-RP channels. Therefore, the received signal is

$$y_i(t) = \sum_{l=1}^{N+K} B_{l,i} g(t - \mu_{l,i}) e^{j\left(\omega(t-\mu_{l,i})+\theta_{l,i}\right)}. \quad (7)$$

B. RSS Model

Equation (7) shows that RIS adds delayed and amplified versions of the originally transmitted signal to an RP. Therefore, at the ith RP,

$$|y_i(t)|^2 = \sum_{l}^{N+K} \sum_{v}^{N+K} B_{l,i} B_{v,i} g(t - \mu_{l,i}) g(t - \mu_{v,i}) e^{j\left(\theta_{l,i}-\theta_{v,i}+\omega(\mu_{v,i}-\mu_{l,i})\right)}, \quad (8)$$

where $\theta_{l,i}$ is a uniformly disturbed random variable. Therefore,

$$E_i(t) = \mathbf{E}_\theta \left\{ |y_i(t)|^2 \right\} = \sum_{l}^{K+N} B_{l,i}^2 g^2(t - \mu_{l,i}), \quad (9)$$

where $\mathbf{E}_\theta \{.\}$ denotes expected value with respect to θ and,

$$E_i = \int_{T_1}^{T_2} E_i(t) dt. \quad (10)$$

In (10), $T1$, $T2$, are the start and end of energy measurement time span and $(T_2 - T_1) < T$. The time interval of measuring signal strength i.e., $T_2 - T_1$, is the key point that enables RIS static reconfiguration.

The measured RSS at the ith RP is modeled as:

$$\dot{\text{RSS}}_i = 20 \log_{10} \left(\sum_{l=1}^{K+N} B_{l,i}^2 \int_{T_1}^{T_2} g^2(t - \mu_{l,i}) \, dt \right) + \xi, \quad (11)$$

where ξ is a random noise term that captures uncertainty in the RSS measurements. This uncertainty arises from three primary sources: (1) *Measurement noise*, such as thermal fluctuations and receiver imperfections; (2) *Shadow fading*, typically modeled as log-normal due to static obstacles like walls or stationary human bodies [31]; and (3) *Dynamic environmental changes*, such as user mobility or the movement of furniture, doors which introduce time-varying disturbances.

Each of these sources is modeled as a zero-mean random variable, and assuming statistical independence among them, they can be aggregated into a unified zero-mean Gaussian noise process:

$$\xi = \xi_{\text{meas}} + \xi_{\text{shadow}} + \xi_{\text{dyn}} \sim \mathcal{N}(0, \sigma^2), \quad (12)$$

where the total variance is given by:

$$\sigma^2 = \sigma^2_{\text{meas}} + \sigma^2_{\text{shadow}} + \bar{\sigma}^2_{\text{dyn}}. \quad (13)$$

Here, $\bar{\sigma}^2_{\text{dyn}}$ denotes the time-averaged variance of the dynamic environmental noise, which may vary non-stationarily over time but is approximated as locally stationary for the purpose of snapshot-based RSS evaluation.

Consequently, the overall measured RSS at RP_i is modeled as a Gaussian random variable with:

$$\dot{\text{RSS}}_i \sim \mathcal{N}(S_i(\mathbf{\Gamma}), \sigma^2), \quad (14)$$

where $S_i(\mathbf{\Gamma})$ represents the expected RSS value determined by the RIS configuration $\mathbf{\Gamma}$.

III. Problem Formulation

Our objective is to assign $S_i(\mathbf{\Gamma})$, The expected RSS values, based on an optimal RSS distribution to enhance localization accuracy. In the following subsection, we show that MDRSS, as an RSS distribution, effectively reduces the localization error.

Lemma: The likelihood of false positioning errors decreases when the observed RSS values are sufficiently distinct between different RPs. Given a uniform prior distribution of user location, the probability of false positioning between two RPs, denoted RP_i and $\text{RP}_{i'}$, is minimized when the observed RSS value lies closer to its true assigned RSS expected value $S_i(\Gamma)$ than to $S_{i'}(\Gamma)$.

Proof: For a given configuration $\mathbf{\Gamma}$, the probability distribution of the RSS value at the ith RP is given by:

$$\mathbb{P}(\dot{\text{RSS}}|S_i(\mathbf{\Gamma}), i) = \frac{1}{\sqrt{2\pi\sigma^2}} e^{-\frac{\left(\dot{\text{RSS}} - S_i(\mathbf{\Gamma})\right)^2}{2\sigma^2}}, \quad (15)$$

which follows a normal distribution. To minimize false positioning between any two arbitrary RPs, i and i', the following condition must hold:

$$\mathbb{P}(i \mid \dot{\text{RSS}}, S_i(\mathbf{\Gamma})) > \mathbb{P}(i' \mid \dot{\text{RSS}}, S_i(\mathbf{\Gamma})), \quad \forall i' \neq i \quad (16)$$

Using Bayes' theorem, the conditional probability is expressed as:

$$\mathbb{P}(i|\dot{\text{RSS}}, S_i(\mathbf{\Gamma})) = \frac{p_i \mathbb{P}(\dot{\text{RSS}}|S_i(\mathbf{\Gamma}), i)}{\sum_j p_j \mathbb{P}(\dot{\text{RSS}}|S_i(\mathbf{\Gamma}), j)}, \tag{17}$$

where p_i represents the user's prior location probability. Under assumption of equal priors (i.e., $p_i = p_{i'}$), the inequality simplifies to a comparison of likelihoods:

$$\frac{1}{\sqrt{2\pi\sigma^2}} e^{-\frac{\left(\dot{\text{RSS}} - S_i(\mathbf{\Gamma})\right)^2}{2\sigma^2}} > \frac{1}{\sqrt{2\pi\sigma^2}} e^{-\frac{\left(\dot{\text{RSS}} - S_{i'}(\mathbf{\Gamma})\right)^2}{2\sigma^2}}, \tag{18}$$

taking logarithms and simplifying:

$$\begin{aligned} &\left(\dot{\text{RSS}} - S_i(\mathbf{\Gamma})\right)^2 < \left(\dot{\text{RSS}} - S_{i'}(\mathbf{\Gamma})\right)^2 \\ \Rightarrow \quad &2\Big(S_{i'}(\mathbf{\Gamma}) - S_i(\mathbf{\Gamma})\Big)\dot{\text{RSS}} < S_{i'}(\mathbf{\Gamma})^2 - S_i(\mathbf{\Gamma})^2. \end{aligned} \tag{19}$$

Hence, the decision boundary is the midpoint:

$$\dot{\text{RSS}} \begin{cases} > \dfrac{S_i(\mathbf{\Gamma}) + S_{i'}(\mathbf{\Gamma})}{2}, & \text{if } S_i(\mathbf{\Gamma}) > S_{i'}(\mathbf{\Gamma}) \\ < \dfrac{S_i(\mathbf{\Gamma}) + S_{i'}(\mathbf{\Gamma})}{2}, & \text{if } S_i(\mathbf{\Gamma}) < S_{i'}(\mathbf{\Gamma}) \end{cases} \tag{20}$$

To ensure reliable positioning, we define a confidence interval radius ς, which represents the maximum acceptable deviation of the observed RSS from its expected value due to multiple sources of signal uncertainty. These include measurement noise, shadow fading, and dynamic environmental variations such as people movement or changes in room layout, which lead to time-varying fluctuations in RSS.

We assume that these uncertainties are statistically independent and homogeneous across RPs, allowing their effects to be combined into a single unified model. This assumption is valid in the context of our proposed system, which targets high-precision localization in relatively small environments such as a room or corridor. Since all RPs are located within the same enclosed space, the physical environment is statistically similar across them. As a result, the probability distributions of RSS disturbances—both static and dynamic—tend to exhibit similar characteristics at different RPs.

In particular, dynamic fluctuations caused by human activity (e.g., a person walking through the environment) typically affect multiple RPs in a statistically comparable manner, even if the exact impact at each point varies. Additionally, because RSS measurements are averaged over short time intervals, it is reasonable to model the dynamic noise as locally stationary. Under this approximation, the variance of RSS fluctuations can be treated as approximately constant across RPs within the measurement window, thereby justifying the use of a homogeneous uncertainty model.

Therefore, the confidence interval ς is used to represent the net uncertainty in the RSS value, capturing approximately 95% of its expected deviation from the mean. This unified modeling enables the derivation of robust decision boundaries for positioning, even in the presence of complex environmental dynamics.

To avoid misclassification between two reference points, RP_i and $\text{RP}_{i'}$, we must ensure that the entire confidence interval around $S_i(\mathbf{\Gamma})$ lies on the correct side of the decision boundary. As established in the previous lemma, this boundary is the midpoint between the expected RSS values:

$$\text{RSS}_{\text{threshold}} = \frac{S_i(\mathbf{\Gamma}) + S_{i'}(\mathbf{\Gamma})}{2}. \tag{21}$$

If $S_i(\mathbf{\Gamma}) < S_{i'}(\mathbf{\Gamma})$, the condition becomes:

$$S_i(\mathbf{\Gamma}) + \varsigma < \frac{S_i(\mathbf{\Gamma}) + S_{i'}(\mathbf{\Gamma})}{2} \Rightarrow \varsigma < \frac{S_{i'}(\mathbf{\Gamma}) - S_i(\mathbf{\Gamma})}{2}. \tag{22}$$

If $S_i(\mathbf{\Gamma}) > S_{i'}(\mathbf{\Gamma})$, we require:

$$S_i(\mathbf{\Gamma}) - \varsigma > \frac{S_i(\mathbf{\Gamma}) + S_{i'}(\mathbf{\Gamma})}{2} \Rightarrow \varsigma < \frac{S_i(\mathbf{\Gamma}) - S_{i'}(\mathbf{\Gamma})}{2}. \tag{23}$$

These two cases can be unified into the following inequality:

$$\varsigma < \frac{|S_i(\mathbf{\Gamma}) - S_{i'}(\mathbf{\Gamma})|}{2}. \tag{24}$$

This upper bound defines the maximum permissible variation in signal strength, denoted by ς, that can be tolerated while maintaining reliable localization performance. In practice, RSS fluctuations in indoor environments typically exhibit a standard deviation between 2 and 6 dB [32], [33] . Therefore, the confidence interval radius ς which corresponds to approximately $\pm 1.96\sigma$ for a 95% confidence level, is expected to range between 4 and 12 dB in most real-world scenarios.

In environments where RSS is affected by multiple sources of uncertainty, an increase in ς implies a higher risk of classification ambiguity. To mitigate this risk, the RSS values assigned to different RPs must be sufficiently distinct. In other words, the greater the separation between the expected RSS values of any two RPs, the more resilient the system becomes to overlapping confidence intervals and misclassification errors.

Therefore, a key design objective of the proposed RIS-assisted system is to maximize the pairwise RSS separation across all RPs. We define this objective as Maximum Differentiated RSS (MDRSS). By maximizing the RSS contrast between RPs, the system improves its robustness not only to measurement noise but also to real-world conditions such as moving users, obstructing objects, and other dynamic changes in the environment, all of which are implicitly captured within the confidence interval ς. ■

A. Assigning MDRSS to the RPs

Here, we analyze the assignment of MDRSS to the RPs within an environment and subsequently present our approach to addressing this problem.

Given that the distance between RIS elements is significantly smaller than the distance between RPs, it is reasonable to treat the RIS as a single-point receiver and transmitter. Consequently, the amplitude coefficients for all RIS elements can be assumed equal for a given RP, leading to the following simplifications: $\alpha'_{1,i} = \alpha'_{2,i} = \cdots = \alpha'_{N,i} = \alpha'_i$, and $\alpha_1 = \alpha_2 = \cdots = \alpha_N = \alpha$. This assumption allows for a more tractable analysis of the RSS assignment and

facilitates the development of a practical solution to the problem. Substituting (5) into (11) yields:

$$\sum_{n=1}^{N} \beta_n^2 \int_{T_1}^{T_2} g^2(t-\mu_{n,i})dt = \left(\frac{1}{\alpha^2 \alpha_i'^2}\right)\left\{10^{\mathrm{RSS}_i/20} - \sum_{k=1}^{K} B_{k,i}^2 \int_{T_1}^{T_2} g^2(t-\mu_{k,i})dt\right\}, \tag{25}$$

or equivalently:

$$\sum_{n=1}^{N} \beta_n^2 \int_{T_1}^{T_2} g^2(t-\mu_{n,i})dt = C_i, \tag{26}$$

where C_i are the values that we aim to adjust to obtain MDRSS. Note that the term $\mu_{n,i}$, representing the total propagation delay experienced by the signal, consists of two components: t_n, which is adjusted by the nth element of the RIS, and $\tau_{n,i} = \tau_n + \tau'_{n,i}$, the delay caused by transferring the wireless signal in an environment.

Generally, the sampling frequency of the wireless signal, f_s, is such that $1/f_s < Dt$, where $Dt = \tau_{u,i} - \tau_{v,i}$, and u and v are any two arbitrary RIS elements. Consequently, signals received at the same RP from different RIS elements experience different delays due to varying t_n values. Similarly, signals received at different RPs from the same RIS element experience different delays due to the varying $\tau_{n,i}$ values. We set $\int_{T_1}^{T_2} g^2(t-\mu_{n,i})dt \triangleq G(\tau_{n,i}, t_n)$, hence,

$$\begin{cases} \beta_1^2 G(\tau_{1,1}, t_1) + \beta_2^2 G(\tau_{2,1}, t_2) + ... + \beta_N^2 G(\tau_{N,1}, t_N) & = C_1 \\ \beta_1^2 G(\tau_{1,2}, t_1) + \beta_2^2 G(\tau_{2,2}, t_2) + ... + \beta_N^2 G(\tau_{N,2}, t_N) & = C_2 \\ & \cdot \\ & \cdot \\ & \cdot \\ \beta_1^2 G(\tau_{1,I}, t_1) + \beta_2^2 G(\tau_{2,I}, t_2) + ... + \beta_N^2 G(\tau_{N,I}, t_N) & = C_I \end{cases}$$

This can be represented as the following matrix equation,

$$\mathbf{G}\boldsymbol{\Upsilon} = \mathbf{C}, \tag{27}$$

hence,

$$\boldsymbol{\Upsilon} = \mathbf{G^{-1}C}, \tag{28}$$

where $\mathbf{G}$ is an $I \times N$ matrix and $\boldsymbol{\Upsilon} = [\beta_1^2, \beta_2^2, \beta_3^2, ..., \beta_N^2]^T$. To solve (28), it is essential to ensure the non-singularity of $\mathbf{G}$ to guarantee the existence of a unique solution. Furthermore, since $\boldsymbol{\Upsilon}$ represents a vector of squared amplitudes, only positive solutions to (28) are physically valid and acceptable.

Given the above formulation, the objective is to determine the optimal configuration of the RIS that customizes the C_i values to achieve the desired MDRSS distribution. This involves determining the appropriate values of β_n and t_n. However, identifying the RIS delays and amplitudes that produce the most distinct RSS values in the radio map typically requires a brute-force search across all possible combinations of the coefficients. Consequently, this problem involves an exhaustive search through all configurations to find an optimal solution, classifying it as an NP-hard problem.

To overcome the impracticality of performing such an exhaustive search, we propose the SRA, which significantly reduces computational complexity while effectively addressing the problem.

IV. Static Reconfiguration algorithm

The Static Reconfiguration Algorithm optimizes RIS configurations across multiple RPs using a single static setup. Users experience pre-optimized signal patterns as they move, eliminating the need for dynamic reconfiguration.

This approach also eliminates restrictions on the number of users the system can support, as the RIS configurations are not tied to individual users but to locations. Moreover, the implementation does not require orthogonal multiplexing access methods, such as Time Division Multiple Access (TDMA), to handle multiple users. However, TDMA can still be employed to enhance diversity and improve localization accuracy, as will be discussed in subsequent sections.

The SRA operates in two key phases. In the first phase, rather than utilizing all RIS elements simultaneously, an exclusive subset of RIS elements is assigned to each RP. These subsets vary between RPs, effectively altering the RIS configuration as a user moves from one RP to another. Each subset includes at least one RIS element with a freely adjustable amplitude, allowing the assignment of the relative C_i to the corresponding RP_i and ensuring the non-singularity of $\mathbf{G}$. By adjusting t_n in this phase, distinct RIS configurations are realized for different RPs. This approach significantly reduces the computational complexity associated with the NP-hard nature of the problem.

In the second phase, the constraints necessary to ensure positive solutions for (28) are determined. These constraints are integrated into the max-min optimization problem to calculate the amplitude coefficients of the RIS elements. This step finalizes the configuration, ensuring the assignment of MDRSS values to the indoor environment. Together, these two phases enable the SRA to efficiently address the problem while maintaining computational traceability.

In the following section, we detail how RIS delay determination is employed to dynamically manage the activation of specific subsets of RIS elements, enabling the achievement of the desired MDRSS at the targeted RPs.

A. Determining RIS Delay

The objective is to assign a unique subset of RIS elements to each RP. For any arbitrary pair of RPs, denoted as (i, j), there exist subsets $\boldsymbol{\nu}_i$ and $\boldsymbol{\nu}_j$ such that:

$$\boldsymbol{\nu}_i \subseteq \boldsymbol{\Upsilon}, \quad \boldsymbol{\nu}_j \subseteq \boldsymbol{\Upsilon}, \quad \boldsymbol{\nu}_i \neq \boldsymbol{\nu}_j,$$

where $\boldsymbol{\nu}_i$ and $\boldsymbol{\nu}_j$ are the sets of RIS elements configured to assign C_i and C_j to RP_i and RP_j, respectively. While each subset $\boldsymbol{\nu}_i$ may include multiple elements, only one element within the subset has an amplitude that can directly control and assign the relative C_i to RP_i. This condition ensures the existence of a solution to the system of equations in (27). We refer to this amplitude-controlling element as the *linked element*. Thus, for each RP, the corresponding linked element

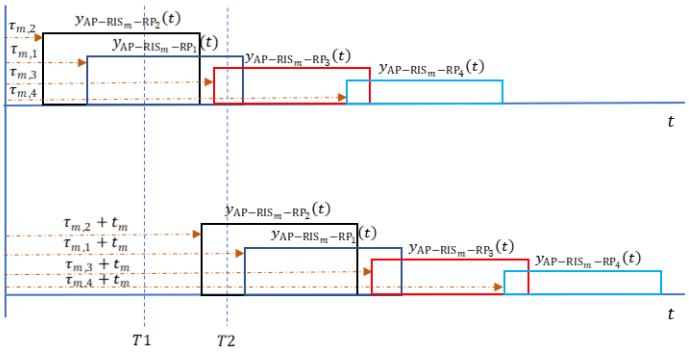

Fig. 2. Illustration of delay adjustment in an RIS element. Initially, four RPs receive signals from the m-th RIS element (top). After adjusting the delay (bottom), only RP2 receives the signal within the measurement window T_1 to T_2.

within the RIS must be identified. It is crucial to establish a one-to-one correspondence between each RP and its linked element to guarantee the feasibility of the configuration in the environment.

Let $\boldsymbol{\mu}_m$ be a vector of delays that includes $\tau_{m,i}$ and t_m:

$$\boldsymbol{\mu}_m \triangleq [t_m + \tau_{m,1}, t_m + \tau_{m,2}, t_m + \tau_{m,3}, \ldots, t_m + \tau_{m,I}]^t,$$

where $\tau_{m,k} = \min_i\{\tau_{m,i}\}$. We then define $\mathbf{G}_{(i,m)}$ as follows:

$$\mathbf{G}_{(i,m)} \triangleq \int_{T_1}^{T_2} g^2(t - \boldsymbol{\mu}_{m(i)})dt. \tag{29}$$

By adjusting t_m such that $t_m + \tau_{m,k} = T_2 - \epsilon$, the mth RIS element can act as a linked element for the kth RP. This is because:

$$\mathbf{G}_{(i,m)} = \begin{cases} \int_{T_2-\epsilon}^{T_2} g^2(t - \boldsymbol{\mu}_{m(k)})dt & \text{if } i = k, \\ 0 & \text{if } i \neq k, \end{cases} \tag{30}$$

where ϵ is chosen such that:

$$\tau_{m,i} + t_m = \begin{cases} < T_2 & \text{if } i = k, \\ \geq T_2 & \text{if } i \neq k. \end{cases} \tag{31}$$

In this method, we select an RP with the minimum propagation delay from a given RIS element compared to all other RPs. By adjusting t_m, the signal is shifted such that it is received exclusively within the energy measurement span of the RP with the minimum propagation delay, ensuring it is not received at any other RPs. Fig. 2 illustrates this procedure.

As shown, after adjusting t_m, the signal received from RIS_m contributes solely to the determination of the RSS at RP_2. Consequently, the amplitude coefficient of RIS_m can be freely adjusted to control the RSS at RP_2. It is important to emphasize that while this guarantees RIS_m is uniquely linked to RP_2, it does not imply that $\boldsymbol{\nu}_2$ comprises only RIS_m. Depending on the time delay adjustments for other RIS elements, additional elements may also contribute to RP_2. However, RIS_m is unequivocally designated as the linked element for RP_2.

Once RIS_m is identified as the linked element for RP_k, it is ensured that no other RIS elements are linked to the same RP. In other words, the objective is to establish a one-to-one correspondence between RIS elements and RPs. As a result, regardless of the total number of RIS elements, only as many elements as there are RPs will ultimately be utilized.

Suppose $\tau_{m,k}$ is the minimum delay of $\boldsymbol{\mu}_m$, which establishes RIS_m as the linked element for RP_k, and $\tau'_{m+1,k}$ is the minimum delay of $\boldsymbol{\mu}_{m+1}$. To avoid linking $\mathrm{RIS}_{(m+1)}$ to RP_k again, instead of setting $t_{m+1} + \tau'_{m+1,k} = T_2 - \epsilon$, we set $t_{m+1} + \tau'_{m+1,k'} = T_2 - \epsilon$, where $\tau'_{m+1,k'}$ is the second minimum delay. Consequently, we have:

$$\mathbf{G}_{(i,m+1)} = \begin{cases} \int_{T_2-\epsilon'}^{T_2} g^2(t - \boldsymbol{\mu}_{m+1(k)})dt & \text{if } i = k, \\ \int_{T_2-\epsilon}^{T_2} g^2(t - \boldsymbol{\mu}_{m+1(k')})dt & \text{if } i = k', \\ 0 & \text{if } i \notin (k, k'), \end{cases} \tag{32}$$

where $\epsilon' = \epsilon + (\tau'_{m+1,k'} - \tau'_{m+1,k})$. With this configuration, while $\mathrm{RIS}_{(m+1)}$ becomes the linked element for $\mathrm{RP}_{k'}$, the vector $\boldsymbol{\nu}_k$ must also be updated to include β^2_{m+1}, ensuring $\beta^2_{m+1} \in \boldsymbol{\nu}_k$.

Similarly, for any mth column of $\mathbf{G}_{(:,m)}$, the nonzero elements are obtained for $i = k$ and for all j such that $\tau_{m,j} \leq \tau_{m,k}$, provided that $k \notin \boldsymbol{\Theta}$, where $\boldsymbol{\Theta}$ is the set of nonzero indices from $\mathbf{G}_{(:,1)}$ to $\mathbf{G}_{(:,m-1)}$. This ensures a one-to-one correspondence between each RP and its linked RIS element, enabling the creation of an exclusive set of corresponding RIS elements for each RP.

The one-to-one correspondence between RIS elements and RPs also results in many elements of $\mathbf{G}$ becoming zero. This sparsity in $\mathbf{G}$ is advantageous as it reduces computational complexity. Specifically, the sparser $\mathbf{G}$ is, the fewer constraints need to be addressed during the optimization phase of the SRA, which will be detailed in the next section. However, achieving greater sparsity in $\mathbf{G}$ requires a larger number of RIS elements.

In cases where $\tau_{(n,k)}$ and $\tau_{(n,j)}$ are the only differing delays between RP_k and RP_j, the nth element of the RIS is utilized as the linked element for either RP_k or RP_j, depending on which RP experiences the shorter delay. Specifically, if $\tau_{(n,k)} < \tau_{(n,j)}$, we set:

$$t_n + \tau_{(n,k)} = T_2 - \epsilon, \tag{33}$$

and define the corresponding elements of $\mathbf{G}_{(i,n)}$ as follow:

$$\mathbf{G}_{(i,n)} = \begin{cases} \int_{T_2-\epsilon'}^{T_2} g^2(t - \boldsymbol{\mu}_{n(i)})dt, & \forall i \mid \tau_{(n,i)} \leq \tau_{(n,k)}, \\ \int_{T_2-\epsilon}^{T_2} g^2(t - \boldsymbol{\mu}_{n(k)})dt, & \text{for } i = k, \\ 0, & \text{otherwise.} \end{cases} \tag{34}$$

This configuration ensures that the nth RIS element is appropriately linked to RP_k, while also accounting for its relationship with other RPs based on the delay conditions.

B. Sparse-Based Linked Element Selection in SRA

Building on the delay design, SRA efficiently assigns each RP a single dominant RIS element, achieving a scalable one-to-one mapping.

Suppose that an indoor environment consists of I RPs. Since one linked element is required for each RP, the algorithm must select I linked elements from among the N available RIS elements. Clearly, $N \geq I$, and the remaining $N - I$ elements can remain inactive. Each RP is thus linked to a single dominant element, ensuring adequate reflection gain while keeping all operations within the far-field regime.

In the SRA, for simplicity and computational efficiency, we priorities the RP–RIS correspondences that produce the sparsest possible measurement matrix $\mathbf{G}$. A sparse $\mathbf{G}$ reduces inter-dependencies between RPs and facilitates low-complexity optimization.

For an arbitrary environment with I RPs and N RIS elements ($N \geq I$), the goal is to establish a sparse correspondence between them. Let the delay matrix be $\boldsymbol{\tau} \in \mathbb{R}^{N\times I}$, where each entry $\tau_{n,i}$ represents the propagation delay between the n-th RIS element and the i-th RP. The SRA identifies a mapping function $\ell(i)$ that assigns each RP i to a unique RIS element by adjusting the element's time delay t_n.

For each RP i, the optimal linked element $n = \ell(i)$ is chosen such that the resulting matrix $\mathbf{G}$ is as sparse as possible. To quantify sparsity, define the set of RPs that receive a nonzero contribution from RIS_n when linked to RP_i as

$$\Omega_n(i) = \{\, j \mid \tau_{n,j} \leq \tau_{n,i} \,\}, \qquad s_{i,n} = |\Omega_n(i)|, \tag{35}$$

here, $s_{i,n}$ measures the nonzero count in column n of $\mathbf{G}$ when RIS_n is linked to RP_i. The SRA then finds an injective mapping ℓ that minimizes the total nonzero count:

$$\ell = \arg \min_{\text{injective } \ell:\{1,\dots,I\}\hookrightarrow\{1,\dots,N\}} \sum_{i=1}^{I} s_{i,\ell(i)}. \tag{36}$$

To further illustrate, consider an indoor environment with $I = 4$ and $N = 4$. Suppose $\tau_{n,i} \in [\tau_1, \tau_2, \tau_3, \tau_4]$, where $\tau_1 < \tau_2 < \tau_3 < \tau_4$. For this environment, we have the following matrix $\boldsymbol{\tau}^T$:

$$\boldsymbol{\tau}^T = \begin{bmatrix} \tau_1 & \tau_2 & \tau_1 & \tau_3 \\ \tau_3 & \tau_4 & \tau_4 & \tau_1 \\ \tau_2 & \tau_2 & \tau_3 & \tau_4 \\ \tau_2 & \tau_3 & \tau_3 & \tau_1 \end{bmatrix}, \tag{37}$$

where $\boldsymbol{\tau}^T$ is the transpose of the matrix $\boldsymbol{\tau}$. If the linked elements for RP_1, RP_2, RP_3, and RP_4 are RIS_1, RIS_4, RIS_2, and RIS_3, respectively, the matrix $\mathbf{G}$ corresponds to:

$$\mathbf{G} = \begin{bmatrix} \mathbf{G}_{(1,1)} & \mathbf{G}_{(1,2)} & \mathbf{G}_{(1,3)} & 0 \\ 0 & 0 & 0 & \mathbf{G}_{(2,4)} \\ 0 & \mathbf{G}_{(3,2)} & \mathbf{G}_{(3,3)} & 0 \\ 0 & 0 & \mathbf{G}_{(4,3)} & \mathbf{G}_{(4,4)} \end{bmatrix}, \tag{38}$$

and the involved RIS elements for each RP are represented as:

$$\boldsymbol{\nu}_1 = [\beta_1^2, \beta_2^2, \beta_3^2], \boldsymbol{\nu}_2 = [\beta_4^2], \boldsymbol{\nu}_3 = [\beta_2^2, \beta_3^2], \boldsymbol{\nu}_4 = [\beta_3^2, \beta_4^2].$$

Alternatively, if the linked elements for RP_1, RP_2, RP_3, and RP_4 are RIS_3, RIS_1, RIS_2, and RIS_4, respectively, the corresponding $\mathbf{G}$ matrix becomes:

$$\mathbf{G} = \begin{bmatrix} \mathbf{G}_{(1,1)} & \mathbf{G}_{(1,2)} & \mathbf{G}_{(1,3)} & 0 \\ \mathbf{G}_{(2,1)} & 0 & 0 & \mathbf{G}_{(2,4)} \\ \mathbf{G}_{(3,1)} & \mathbf{G}_{(3,2)} & 0 & 0 \\ \mathbf{G}_{(4,1)} & \mathbf{G}_{(4,2)} & 0 & \mathbf{G}_{(4,4)} \end{bmatrix}, \tag{39}$$

and the involved RIS elements are:

$$\boldsymbol{\nu}_1 = [\beta_1^2, \beta_2^2, \beta_3^2], \quad \boldsymbol{\nu}_2 = [\beta_1^2, \beta_4^2],$$
$$\boldsymbol{\nu}_3 = [\beta_1^2, \beta_2^2], \quad \boldsymbol{\nu}_4 = [\beta_1^2, \beta_2^2, \beta_4^2].$$

This example demonstrates that different configurations can be applied to the RIS while still achieving the MDRSS in the environment by solving the optimization problem. However, SRA will prioritize configurations that result in the sparsest $\mathbf{G}$ matrix. This approach is formally presented in Algorithm 1.

In the above example, suppose that N extends to 8, with 4 additional RIS elements available for incorporation into the SRA. The updated matrix $\boldsymbol{\tau}^T$ can be represented as:

$$\boldsymbol{\tau}^T = \left[\begin{array}{cccc|cccc} \tau_1 & \tau_2 & \tau_1 & \tau_3 & \tau_2 & \tau_2 & \tau_3 & \tau_2 \\ \tau_3 & \tau_4 & \tau_4 & \tau_1 & \tau_3 & \tau_3 & \tau_4 & \tau_1 \\ \tau_2 & \tau_2 & \tau_3 & \tau_4 & \tau_3 & \tau_2 & \tau_3 & \tau_4 \\ \tau_2 & \tau_3 & \tau_3 & \tau_1 & \tau_4 & \tau_4 & \tau_2 & \tau_4, \end{array}\right], \tag{40}$$

where the vertical bar indicates the separation between the original and additional elements. Using the sparsity-based selection approach of SRA, the linked elements for RP_1, RP_2, RP_3, and RP_4 are RIS_1, RIS_8, RIS_2, and RIS_7, respectively. This configuration results in the following sparse matrix $\mathbf{G}$:

$$\mathbf{G} = \begin{bmatrix} \mathbf{G}_{(1,1)} & \mathbf{G}_{(1,2)} & 0 & 0 & 0 & 0 & 0 & 0 \\ 0 & 0 & 0 & 0 & 0 & 0 & 0 & \mathbf{G}_{(2,8)} \\ 0 & \mathbf{G}_{(3,2)} & 0 & 0 & 0 & 0 & 0 & 0 \\ 0 & 0 & 0 & 0 & 0 & 0 & \mathbf{G}_{(4,7)} & 0 \end{bmatrix}, \tag{41}$$

and the involved elements for each RP are represented as:

$$\boldsymbol{\nu}_1 = [\beta_1^2, \beta_2^2], \boldsymbol{\nu}_2 = [\beta_8^2], \boldsymbol{\nu}_3 = [\beta_2^2], \boldsymbol{\nu}_4 = [\beta_7^2].$$

Clearly, increasing the number of RIS elements allows for greater sparsity in $\mathbf{G}$. As explained, a sparser $\mathbf{G}$ reduces computational complexity by requiring fewer constraints to be defined during the optimization phase of the SRA. Additionally, reducing the number of involved elements for each RP minimizes coupling effects between RIS elements, improving the accuracy of RSS customization for the environment's RPs.

Since only I active RIS elements are needed, the remaining $N - I$ elements can be excluded from the calculations by setting their corresponding entries in $\mathbf{G}$ to zero. Practically, this is equivalent to deactivating those elements or setting their amplitude coefficients to zero.

C. Obtaining C_i

While $\mathbf{G}$ is transformed into a solvable sparse matrix, enabling the matrix equation in (27) to be solved efficiently without resorting to brute-force search methods, customizing

Algorithm 1: Time Shift Determination and Linked Element Selection in SRA

Input: Matrix $\boldsymbol{\tau}$ containing all $\tau_{n,i}$ values, and vector $\boldsymbol{\mu}_n$.
Output: Vector $\mathbf{t}$ containing time shifts for $n = 1 : N$ RIS elements, and matrix $\mathbf{G}$.
Initialize: $min = \infty$, $\mathbf{G} = \text{zeros}(I \times N)$, $\boldsymbol{\tau}_1 = \boldsymbol{\tau}^T$, and $\mathbf{t} = \text{zeros}(1, N)$.
For $i = 1 : I$ **do**
1) **For** $n = 1 : N$ **do**
   a) $NoneZeroElements = \text{find}(\boldsymbol{\tau}_1(:, n) \leq \boldsymbol{\tau}_1(i, n))$
   b) **If** length$(NoneZeroElements) < min$ **then**
      i) $min = \text{length}(NoneZeroElements)$
      ii) $LE = n$ (Set LE as the linked element)
      iii) $mindelay = \boldsymbol{\tau}_1(i, n)$
      End If
   End For
2) **Set** $t_{LE} = T2 - mindelay - \epsilon$
3) **Update** vector $\boldsymbol{\mu}_{LE}$ with the obtained t_{LE}
4) **For any** $\boldsymbol{\mu}_{LE}(i)$ **where** $\boldsymbol{\mu}_{LE}(i) \leq T2$ **do**
   a) $\mathbf{G}_{i,LE} = G(\tau_{LE,i}, t_{LE})$
   b) **Update** $\boldsymbol{\tau}_1(:, LE) = \infty$ (Mark as processed)
   End For
End For

the environment with MDRSS requires SRA to advance to the second step. This step entails solving an optimization problem designed to maximize the minimum Euclidean distance between the RSS values in the environment. By addressing this optimization, the RSS values are distributed with maximum differentiation, ensuring a well-structured environment. Specifically, SRA aims to determine C_i values that achieve MDRSS by considering the squared values of $\boldsymbol{\Upsilon}$, subject to the constraint $\boldsymbol{\Upsilon} > 0$. Consider the vector of RSS values for an environment, represented as $[\text{RSS}_1, \text{RSS}_2, \ldots, \text{RSS}_I]^t$. To achieve MDRSS, the following optimization problem must be solved:

$$\max_{C_i} \min \left\{ \left| \sum_{i=1}^{I} \mathbf{f}_{1,i} \text{RSS}_i \right|, \left| \sum_{i=1}^{I} \mathbf{f}_{2,i} \text{RSS}_i \right| \cdots, \left| \sum_{i=1}^{I} \mathbf{f}_{L,i} \text{RSS}_i, \right| \right\}$$
$$\text{subject to: } lb \leq \text{RSS}_i \leq ub. \tag{42}$$

In the above, lb and ub denote the lower and upper bounds of the RSS_i measurement range, respectively. The matrix $\mathbf{f}$ is of dimensions $L \times I$, where each row consists of exactly one pair of elements: 1 and -1. It is ensured that no two rows of $\mathbf{f}$ are identical. Furthermore, L is constrained to $I - 1$ to enforce minimum distances between neighboring RSS values. For instance, in an environment with four RPs, the ordering $\text{RSS}_1 > \text{RSS}_2 > \text{RSS}_3 > \text{RSS}_4$ illustrates this principle, hence

$$\mathbf{f} = \begin{bmatrix} 1 & -1 & 0 & 0 \\ 0 & 1 & -1 & 0 \\ 0 & 0 & 1 & -1 \end{bmatrix}. \tag{43}$$

The optimization problem in (42) can be reformulated as follows:

$$\max_{C_i} \min \left\{ \left| \mathbf{f}.\ 20\text{log10}\left([C_1, C_2, ..., C_I]^T \right) \right| \right\},$$
$$\text{subject to: } a_i \leq C_i \leq b_i, \tag{44}$$

where

$$a_i = \frac{10^{lb/20} - \sum_k B_{k,i}^2 \int_{T1}^{T2} g^2(t - \mu_{k,i}) dt}{\alpha_i'^2 \alpha^2}, \tag{45}$$

and

$$b_i = \frac{10^{ub/20} - \sum_k B_{k,i}^2 \int_{T1}^{T2} g^2(t - \mu_{k,i}) dt}{\alpha_i'^2 \alpha^2}. \tag{46}$$

In addition to the constraints on C_i outlined above, further constraints on equation (42) are required to guarantee a positive solution. Leveraging the sparse-based computation of $\mathbf{G}$ proves advantageous in this context, as it not only reduces computational complexity but also minimizes the number of necessary constraints.

Let $\boldsymbol{\nu}_i$ denote a subset of $\boldsymbol{\Upsilon}$, representing the elements of the RIS involved in determining the RSS for the ith RP. Then,

$$\text{If} \quad \exists \quad j \in I \ \& \ j \neq i, \ \boldsymbol{\nu}_j \subset \boldsymbol{\nu}_i \xrightarrow{\text{then}} C_i > C_j.$$

For any $\boldsymbol{\nu}_j \subset \boldsymbol{\nu}_i$, the condition of $\boldsymbol{\Upsilon} > 0$ results in

$$\mathbf{G}_{i,:}\boldsymbol{\Upsilon} - \mathbf{G}_{j,:}\boldsymbol{\Upsilon} > 0, \tag{47}$$

where $\mathbf{G}_{i,:}$ is the ith row of matrix $\mathbf{G}$. Also, if there exists an h so that $\boldsymbol{\nu}_h \subset \boldsymbol{\nu}_i$ and $\mathbf{G}_{i,:}\boldsymbol{\Upsilon} - \mathbf{G}_{j,:}\boldsymbol{\Upsilon} - \mathbf{G}_{h,:}\boldsymbol{\Upsilon} > 0$, then

$$C_i > C_j + C_h. \tag{48}$$

Suppose that $\boldsymbol{\Psi}$ stands for a set of indexes of $\boldsymbol{\nu}_i$'s subset. For instance, if $\boldsymbol{\nu}_1$ and $\boldsymbol{\nu}_2$ are $\boldsymbol{\nu}_i$'s subsets then, $\boldsymbol{\Psi}$ corresponds to $\{\{1\}, \{2\}, \{1, 2\}\}$ and $\boldsymbol{\nu}_{\boldsymbol{\Psi}_{j,p}} \subset \boldsymbol{\nu}_i$, where $1 \leq p \leq P_j$ and P_j is the length of $\boldsymbol{\Psi}_j$. Then for any $\boldsymbol{\Psi}_j$:

$$if \quad \mathbf{G}_{i,:}\boldsymbol{\Upsilon} - \textstyle\sum_{p=1}^{P_j} \mathbf{G}_{\boldsymbol{\Psi}_{j,p},:}\boldsymbol{\Upsilon} > 0 \quad \Rightarrow \quad C_i > \textstyle\sum_{p=1}^{P_j} C_{\boldsymbol{\Psi}_{j,p}}.$$

To guarantee a positive solution for $\boldsymbol{\Upsilon}$, the constraints on C_i must be satisfied. These constraints can be effectively represented in the relative framework of the matrix $\mathbf{A}$. Consequently, the optimization problem can be formulated as follows:

$$\max_{C_i} \left\{ \min \left\{ \left| \mathbf{f}.\ 20\text{log10}\left([C_1, C_2, ..., C_I]^T \right) \right| \right\} \right\},$$
$$\text{subject to: } a_i \leq C_i \leq b_i, \ \mathbf{A} \times \mathbf{C} < 0, \tag{49}$$

where $\mathbf{C} = [C_1, C_2, \ldots, C_I]^T$. The optimization problem in (49) is solved using Sequential Quadratic Programming (SQP) [16]. However, in practice, the optimizer may converge prematurely, particularly when several C_i values become clustered. In such scenarios, small variations in the RIS configuration $\boldsymbol{\Gamma}$ have little influence on the minimum difference objective. As a result, the SQP algorithm may interpret the solution as optimal and stop the search, even though better configurations may still exist in other regions of the search space.

This article has been accepted for publication in IEEE Transactions on Wireless Communications. This is the author's version which has not been fully edited and content may change prior to final publication. Citation information: DOI 10.1109/TWC.2025.3649587

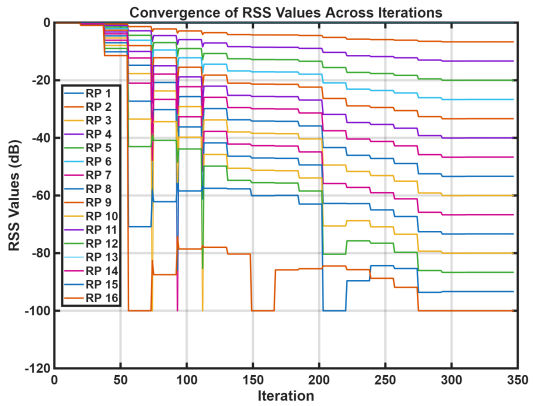

Fig. 3. Convergence of RSS values across iterations for a 4×4 grid with 16 RPs. The SRA algorithm consistently spreads RSS over the 0 dB to -100 dB range.

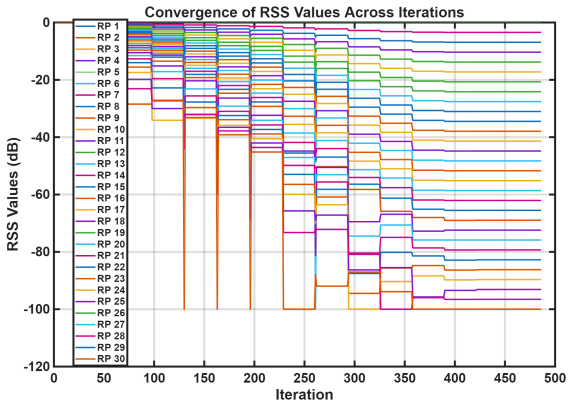

Fig. 4. Convergence of RSS values across iterations for a 6×5 grid with 30 RPs. The SRA algorithm consistently spreads RSS over the 0 dB to -100 dB range with large pairwise differences.

To address this, we modify the objective function by incorporating a mild regularization term that encourages diversity in the expected RSS value profile. This is implemented by subtracting a scaled variance term from the main objective, yielding:

$$\mathbf{fval} = \mathbf{f} \cdot 20\log_{10}(\mathbf{C}) - \lambda \cdot \mathrm{Var}\left(\mathrm{sort}\left(20\log_{10}(\mathbf{C})\right)\right), \quad (50)$$

where λ is a small regularization coefficient (e.g., $\lambda = 0.01$). This formulation discourages degenerate solutions where many C_i values converge to a narrow range and instead steers the optimizer toward configurations that achieve wider RSS separability between RPs.

Although the initial point is set to be fixed as a uniform vector on the upper bound in linear scale, the regularized cost surface enables the algorithm to explore more effective regions of the solution space.

This strategy enhances convergence reliability and generalization to larger or more irregular indoor layouts, Fig. 3 and Fig. 4 represent the convergence pattern of RSS values convergence to the maximum distributed RSS values in the environments with different numbers of RPs.

The effectiveness of the proposed method is illustrated in Fig. 5, comparing radio maps in a 2×2 m indoor area with and without RIS. With RIS and the SRA algorithm, the RSS values exhibit strong spatial diversity and distinguishability across reference points. In contrast, the non-RIS setup shows high spatial correlation, limiting RSS discriminability and impairing localization accuracy. Once the C_i values are determined, $\boldsymbol{\Upsilon}$ is calculated via (28), enabling a tailored RIS configuration using the computed $\mathbf{t}_m$ and $\boldsymbol{\Upsilon}$. During localization, user RSS readings under the SRA scheme are processed using Nearest Neighbor classification to estimate the user's position.

Furthermore, to highlight the advantage of the proposed SRA over non-optimized RIS configurations, Fig. 6 compares the RSS heatmaps obtained under two RIS-aided scenarios: the proposed SRA-optimized configuration and a randomly initialized RIS setup. While both cases leverage RIS-assisted reflection, the random configuration produces highly irregular and spatially biased RSS distributions, resulting in poor correlation between spatial position and signal strength. In contrast, the SRA achieves a smoother and more spatially distinctive RSS pattern, which enhances localization discriminability and reduces ambiguity across RPs.

D. Complexity and Scalability Analysis of SRA

A key advantage of the proposed SRA-based IPS lies in its decoupled architecture: RIS configurations are computed offline, eliminating the need for real-time, user-specific updates. This design ensures scalability, as additional users can be supported without incurring extra optimization overhead. In contrast, per-slot dynamic RIS control, as reported in [34], significantly increases runtime complexity and signaling overhead in mobile edge computing environments.

Despite its static nature, the system remains robust in dynamic settings due to the MDRSS principle, which maximizes RSS separation among RPs. This enhances resilience to disturbances like user movement or layout changes. Such effects are modeled as bounded uncertainties, and well-separated RSS values reduce the risk of localization errors.

However, there is a trade-off: increasing the number of RPs in a fixed RSS range (e.g. –100 dB to 0 dB) compresses the available space between RSS values. This limits the system's tolerance to noise, as shown by comparing Fig. 3 and Fig. 4.

However, to address the limitations that arise when the environment includes a larger number of RPs, our approach leverages RIS reconfiguration to expand the effective RSS feature space. This allows for maintaining sufficient signal differentiation even as the number of RP grows. This will be further discussed in multidimensional RSS design for accuracy improvement section.

E. Computational Complexity Analysis

To assess the computational efficiency of SRA, we break down its main steps and compare the complexity with recent dynamic RIS methods such as Metalocalization [35].

SRA includes two stages: first, constructing the matrix $\mathbf{G}$ where, for each of the I reference points, one RIS element is selected from N candidates, leading to a complexity of $\mathcal{O}(I \cdot N)$. The result is a square $\mathbf{G}$ matrix of size $I \times I$, which streamlines the subsequent optimization. Second,

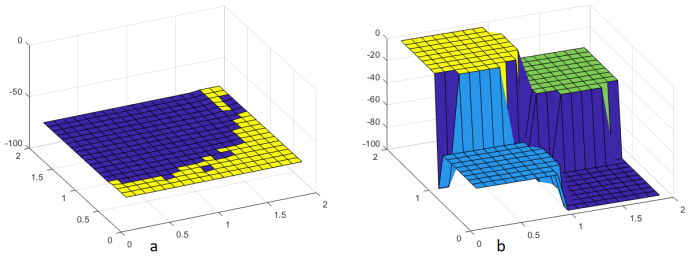

Fig. 5. (a) Radio map of a $2 \times 2m$ indoor environment without RIS, and (b) with RIS. With SRA, the environment leverages an expanded RSS range (-100 dB to 0 dB) and maximizes the RSS disparity between neighboring RPs, significantly improving differentiation and localization accuracy.

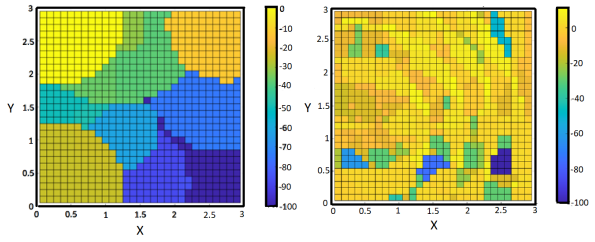

Fig. 6. Comparison of RIS-aided RSS heatmaps: Left, proposed SRA-optimized configuration. Right, random RIS configuration. The SRA produces a smoother and more spatially diverse RSS distribution, enhancing localization resolution compared with the random setup.

solving a constrained max–min optimization problem with regularization to diversify RSS values across RPs. This stage solves for the optimal RSS distribution using SQP with I variables, resulting in a complexity of $\mathcal{O}(I^2 \cdot \text{Iter}_{\text{SQP}})$, where Iter_{SQP} is the number of SQP iterations.

Therefore, the total computational complexity of SRA is:

$$\mathcal{O}(I \cdot N + I^2 \cdot \text{Iter}_{\text{SQP}}). \tag{51}$$

The MetaLocalization framework, in contrast, relies on dynamic reconfiguration of the RIS using Phase shift Optimization (PSO), which operates on a per-user basis. Its reported computational complexity is significantly higher:

$$\mathcal{O}\left((Z_u+1)I^2MN^3 + (Z_u+1-Z_l)CIN^2\right), \tag{52}$$

where I is the number of users, N is the number of RPs, M is the number of RIS elements, C is the number of phase shifts, and Z_u, Z_l are search granularity levels.

SRA algorithm offers significantly lower computational complexity compared to the MetaLocalization framework. While MetaLocalization incurs a high computational burden due to per-user phase shift optimization across a large RIS configuration space, SRA performs a one-time RIS element selection and a centralized max–min optimization over a reduced $I \times I$ matrix. Specifically, SRA's complexity scales as $\mathcal{O}(I \cdot N + I^2 \cdot \text{Iter}_{\text{SQP}})$, which is polynomial and independent of the number of users or RIS phase shifts. In contrast, MetaLocalization's complexity grows steeply as $\mathcal{O}((Z_u + 1)I^2MN^3 + (Z_u + 1 - Z_l)CIN^2)$, with additional dependence on fine-grained user feedback and adaptive reconfiguration. This makes SRA a scalable and practical choice for real-time indoor localization scenarios.

To evaluate the scalability and computational robustness of the proposed SRA, we conducted a series of tests across environments with varying room sizes, numbers of RPs, and RIS elements. For each configuration, we measured the average optimization time. These experiments allow us to analyze how the algorithm performs as the environment grows in size and complexity, and to verify that it maintains acceptable convergence behavior and computational efficiency. The results presented in Table I, confirm that the SRA framework scales reliably with different number of RPs and RIS elements.

TABLE I
AVERAGE EXECUTION TIME OF THE SRA OPTIMIZATION UNDER DIFFERENT ENVIRONMENT SCALES.

Room Size (m)	RPs (I)	RIS Elements (N)	Avg. Time (s)
2×2	4	4	0.49
4×4	16	20	2.35
4×3 (L shape)	7	16	1.67
4×2	8	25	1.87
5×2	40	64	2.5
6×5	30	64	5.33

V. MULTIDIMENSIONAL RSS DESIGN FOR ACCURACY IMPROVEMENT

Conventionally, to enhance localization accuracy, multiple APs are utilized to generate a vector of RSS values for a RP instead of relying on a single RSS value. Extending the dimensions of RSS measurements expands the decision space during the localization phase. For example, adding one additional RSS measurement can result in up to a 40% increase in the maximum Euclidean distance. In higher-dimensional spaces, the differences between RSS vectors (e.g., Euclidean distance) provide more distinguishable metrics for positioning.

As described, SRA does not require time multiplexing to support multiple users due to its reliance on static reconfiguration. This allows time-division multiplexing to be further leveraged to improve localization accuracy. We argue that SRA takes advantage of time diversity to expand the dimensions of RSS measurements, thereby significantly enhancing positioning accuracy.

The RIS operates to customize MDRSS within a time slot $[T_1, T_2]$. By adopting the Time Division Multiplexing (TDM) technique, SRA leverages measurements from different time slots to add additional dimensions to the RSS vector. Let $R_i = [\text{RSS}_{(i,1)}, \text{RSS}_{(i,2)}, \ldots, \text{RSS}_{(i,r)}]$ represent a vector of r measured RSS values, where $\text{RSS}_{(i,r)}$ corresponds to the RSS value of the ith reference point (RP) measured during the rth time slot. Each time slot has a fixed duration dedicated to measuring the signal strength, starting after a short guard time following the conclusion of the $(r-1)$th time slot. Consequently, (27) can be reformulated as: $\mathrm{G}^r \boldsymbol{\Upsilon} = \mathbf{C}^r$, where

$$\mathbf{C}^r = [C_{(1,r)}, C_{(2,r)}, ..., C_{(I,r)}]^T,$$

$$\mathbf{G}^r_{(i,m)} = \int_{T_r} g^2\big(t - \mu^r_m(i)\big),$$

and

$$\mu^r_m(i) = t^r_m + \tau_{(m,i)},$$

This article has been accepted for publication in IEEE Transactions on Wireless Communications. This is the author's version which has not been fully edited and content may change prior to final publication. Citation information: DOI 10.1109/TWC.2025.3649587

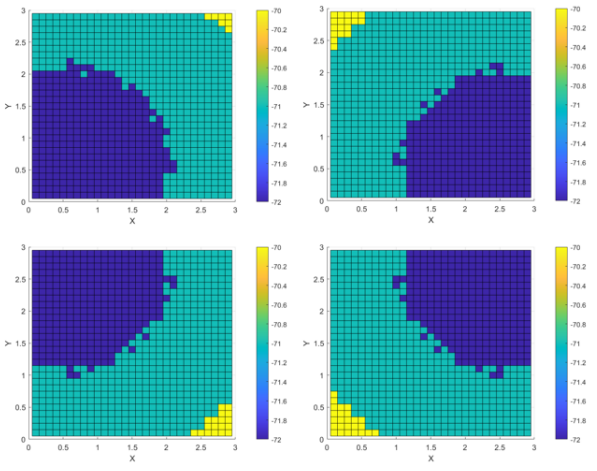

Fig. 7. RSS heatmap without RIS for APs located in 4 corners of a 3 m $\times$ 3 m indoor environment.

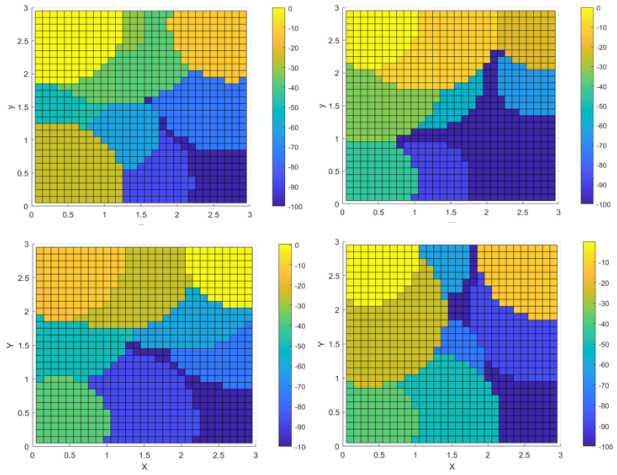

Fig. 8. RSS heatmap with RIS for APs located in 4 corners of a 3 m $\times$ 3 m indoor environment.

Here, T_r represents the rth time slot, and t_m^r denotes the RIS time shift of the mth element during the rth time slot. Solving (V) for each time slot yields the corresponding RIS configuration required for designing the multidimensional RSS of the environment.

The implementation of multiple RSS measurements using time division can be achieved in two ways: (1) by employing a single AP in the environment that transmits its signal to the user via the RIS in different time slots, or (2) by utilizing multiple APs that transmit their signals to the user in distinct, allocated time slots.

In the first scenario, referred to as Single AP Multiple Dimension (SAMD), the key advantage is that transforming a single RSS value into a vector of measurements does not increase the complexity of offline fingerprinting. This is because $\tau_{(m,i)}$ remains constant across all time slots, and the subset of RIS elements determined by SRA for each reference point (RP) is consistent across time slots. Consequently, $C_{(i,1)} = C_{(i,2)} = \cdots = C_{(i,r)}$, while $t_m^1 \neq t_m^2 \neq \ldots \neq t_m^r$. Thus, measuring the RSS for a single time slot during the offline phase is sufficient, as the RSS values for the other time slots can be inferred. However, this approach does not achieve the maximum possible increase in Euclidean distance.

In the second scenario, known as Multiple APs Multiple Dimension (MAMD), the subsets of RIS elements involved for each RP vary across time slots due to the differing positions of the APs. As a result, $C_{(i,1)} \neq C_{(i,2)} \neq \ldots \neq C_{(i,r)}$. This approach offers the potential for higher Euclidean distances, which can significantly improve positioning accuracy.

Figures 7 and 8 show the RSS heatmaps, highlighting the enhanced spatial variation introduced by the RIS configuration. The conventional setup exhibits limited variation (-72 to -70dB), whereas the SRA spreads signal strength from -100 to 0dB, enhancing location separability.

A. Comparison with MDRSS–Dynamic Methods (discussion)

MDRSS–dynamic methods actively time–vary the RIS (or beam/code states) over a short horizon to acquire a T-slot fingerprint

$$\bar{\mathbf{s}}_i \triangleq \left[\mathbf{s}_i(\Theta_1)^\top, \ldots, \mathbf{s}_i(\Theta_T)^\top\right]^\top,$$

whose pairwise distances are typically larger than those obtained under any single configuration. Representative approaches include per-user phase/code scheduling (e.g., "MetaLocalization") and concatenating RSS collected under multiple RIS states or "coded environments" [35]–[37]. A common design formalization is

$$\max_{\Theta_{1:T}} \min_{i \neq j} \left\|\bar{\mathbf{s}}_i - \bar{\mathbf{s}}_j\right\|_2 \quad \text{s.t. hardware/switching constraints,} \tag{53}$$

where Θ_t denotes the RIS state in slot t.

Our SRA targets the complementary point on this spectrum: a *static*, one-shot MDRSS configuration that enlarges inter-RP margins *without* per-user reconfiguration, feedback, or fast RIS switching. A direct numerical bake-off with dynamic schedules is not methodologically neutral unless one *matches latency and control budgets*. Under a simple additive-noise model with slot-independent perturbations, stacking T slots increases the expected Euclidean separation at most on the order of $\sqrt{T}$ (norm growth), while the measurement time and control overhead scale $\propto T$. This trade-off is consistent with our multidimensional analyses (SAMD/MAMD): adding time/AP dimensions monotonically increases separability and improves localization accuracy by expanding the RSS feature space, yet introduces additional acquisition cost (see Secs. V–VI, e.g., Figs. 9–12).

From a deployment standpoint, dynamic schedules typically require (i) fast RIS update rates and tight synchronization; (ii) per-user or per-region adaptation (often PSO/GA or learning-based search); and (iii) time-division operation for multi-user access, all of which impact scalability [35]. By contrast, SRA attains competitive accuracy with a one-time optimization (Sec. IV-D), modest computational cost, and no dynamic control channel during inference. We therefore view static SRA and MDRSS–dynamic methods as *complementary operating points*; a fair head-to-head comparison should be

TABLE II
SIMULATION PARAMETERS

Parameter	Value
Room dimensions	$3 \times 3\,\mathrm{m}^2$ (unless specified)
Grid resolution	$1 \times 1\,\mathrm{m}^2$ per RP (unless specified)
Number of RPs	9 (unless specified)
Number of RIS elements	16 (unless specified)
RIS placement	Ceiling at $z = 3$
RIS origin	$(0.3, 0.3, 3)$
RIS element layout	Square, variable count
Access point	$(0.1, 0.2, 1)$ for single-AP
Multi-AP positions	Corners: $(2.9, 0.1, 1)$, $(0.1, 2.9, 1)$, $(2.9, 2.9, 1)$
Number of multipaths	6 (walls, ceiling, floor) + LoS
Pulse width	10 ns
Carrier frequency	2.4 GHz
Noise model	Additive white Gaussian noise
Power gains	All set to 1
Localization metric	Mean Euclidean error (Eq. (54))

conducted under a matched *error–latency–overhead* protocol, which we leave as scoped future work.

VI. SIMULATION RESULTS

In this section, we evaluate the performance of the proposed RIS-aided indoor positioning system under various simulated scenarios. The core simulation parameters are summarized in Table II for clarity.

The simulated environment consists of a square room with dimensions $3\,\mathrm{m} \times 3\,\mathrm{m}$, divided into 9 reference points (RPs), each covering $1\,\mathrm{m}^2$. The bottom-left corner is set as the origin $(0, 0, 0)$ in a 3D coordinate system. In single AP and SAMD, AP is located at $(0.1, 0.2, 1)$, while in MAMD simulations, three additional APs are placed at $(2.9, 0.1, 1)$, $(0.1, 2.9, 1)$, and $(2.9, 2.9, 1)$.

The RIS is placed horizontally on the ceiling at height $z = 3$, with its bottom-left corner at $(0.3, 0.3, 3)$. It consists of square elements with adjustable center-to-center spacing. The environment includes the LoS path and six multipath reflections (four walls, ceiling, floor). Gaussian noise is added to all RSS readings.

The transmitted pulse width is $w = 10 \times 10^{-9}\,\mathrm{s}$, and signal strength combines the LoS, multipath, and RIS components. All path gain coefficients are set to 1. The positioning error is computed as:

$$P_e = \frac{1}{H} \sum_{h \in H} \left\| p_h^e - p_h^g \right\|, \tag{54}$$

where p_h^e and p_h^g are the estimated and ground-truth positions respectively, and H is the number of Monte Carlo iterations.

We further evaluate positioning accuracy under various system settings, analyzing key parameters such as RSS standard deviation (to assess performance in noisy and dynamic environments), comparison of the multidimensional SRA approach with one-dimensional and conventional fingerprinting methods, RSS measurement range and number of RIS elements. First, the performance of the proposed SRA is compared with the conventional RSS fingerprinting approach. The conventional method uses the NN algorithm to match the location of a user with the closest premeasured

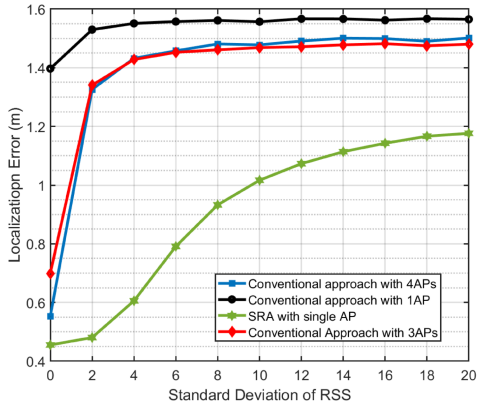

Fig. 9. Comparison of localization errors between the SRA interacting with a single AP and the conventional approach, evaluated in both single-AP and multi-AP scenarios.

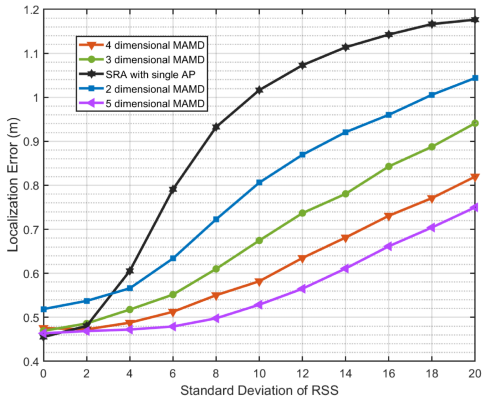

Fig. 10. Comparison of localization accuracy for multidimensional approaches in the SRA and MAMD scenarios.

RSS fingerprints. In our comparison, SRA with a single AP is evaluated against the conventional approach utilizing 1, 3, and 4 APs. The RIS consists of 4×4 elements, with neighboring elements spaced 0.8 m apart. For both SRA and the conventional approach, the RSS measurement range is set between -100 and 0 dB.

The standard deviation of the received signal strength (RSS) is varied from 0 to 20dB to simulate different levels of measurement noise, shadowing, and dynamic fluctuations commonly encountered in indoor environments. Positioning errors are then analyzed under these varying noise conditions. As illustrated in Fig. 9, the proposed SRA method exhibits strong robustness, maintaining high positioning accuracy even at elevated noise levels. Remarkably, SRA achieves superior localization performance using only a single AP, outperforming conventional systems that rely on multiple APs.

Under similar simulation settings, Fig. 10 illustrates the accuracy improvements achieved by the proposed multidimensional SRA in the MAMD configuration. In this analysis, 1 to 5 APs were strategically placed at distinct locations, with one AP location selected randomly. The results clearly demonstrate that increasing the dimensionality of the RSS by incorporating measurements from additional APs consistently enhances localization accuracy. This

This article has been accepted for publication in IEEE Transactions on Wireless Communications. This is the author's version which has not been fully edited and content may change prior to final publication. Citation information: DOI 10.1109/TWC.2025.3649587

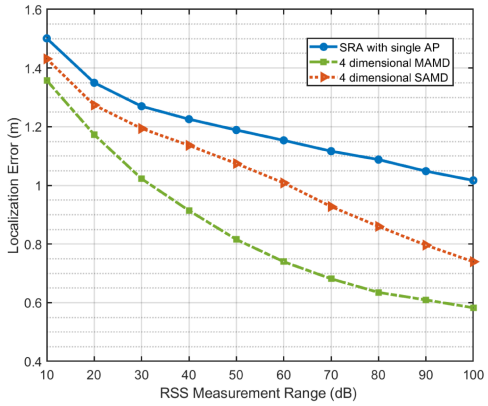

Fig. 11. Comparison of localization errors for multidimensional SRA across different RSS measurement ranges with a standard deviation of 10.

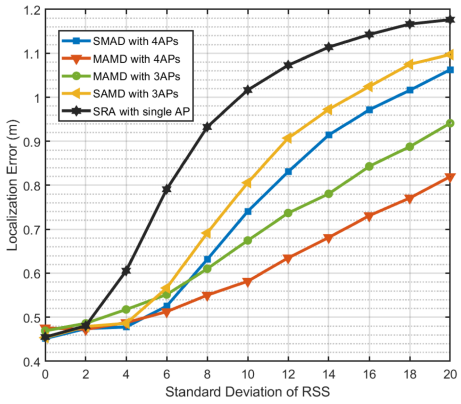

Fig. 12. Comparison of localization errors between the SAMD and MAMD approaches.

improvement is attributed to the time-division multiplexing and reconfiguration capabilities of the RIS, which effectively improve positioning robustness and precision.

Additionally, the ability to preserve the RIS reconfiguration property for accuracy—enabled by the static reconfiguration inherent in SRA allows our approach to maintain superior accuracy even in highly noisy environments. While spatial correlation in the RSS of closely located areas limits accuracy improvements in the multidimensional conventional approach, the multidimensional SRA overcomes these challenges and significantly enhances positioning accuracy. Furthermore, as long as more diverse RSS distributions are leveraged through additional dimensions, greater accuracy can be achieved.

Figure 11 illustrates the impact of varying the RSS measurement range on positioning accuracy, with the RSS standard deviation fixed at 10. The results clearly show that a wider measurement range improves system accuracy. This improvement occurs because a broader range increases the maximum differences in RSS values between neighboring RPs, thereby reducing the likelihood of false positioning. For instance, in the measurement range of $(-25, 0)$ dB, the maximum difference in RSS values between neighboring RPs is approximately $\left|\frac{-25-0}{9}\right| \simeq 2.8$, while it increases to 11.11 in the range of $(-100, 0)$ dB. Consequently, a wider measurement range not only enhances the system's ability to handle higher noise levels but also promotes more diverse RSS distributions among RPs.

Figure 12 illustrates a comparison of the multidimensional MAMD, SAMD, and single AP SRA approaches. As anticipated, the SAMD approach offers smaller Euclidean distances compared to MAMD, resulting in a comparatively lower accuracy improvement. However, similar to multidimensional MAMD, the SAMD approach demonstrates enhanced accuracy and effectively mitigates the impact of spatial correlation in noisy environments. Furthermore, increasing the dimensionality in SAMD results in additional accuracy improvements.

To assess the generality and scalability of SRA, simulations were performed across various indoor layouts, including square, rectangular, L-shaped, and corridor environments with differing room sizes, numbers of RPs, and RIS elements. Scenarios ranged from single- to multi-AP setups to evaluate both baseline and multidimensional configurations. As shown in Fig. 13, SRA consistently maintained strong spatial discrimination and localization accuracy across all geometries.

Obviously, the performance of SRA is closely linked to the number of RPs. As the number of reference points increases, the RSS separability between RPs may diminish, the Multidimensional SRA (MAMD) configuration, which leverages multiple APs and the reconfigurable properties of the RIS, can effectively compensate for performance losses; however, it is worth noting that SRA is scoped toward small-to-moderate indoor environments.

A. *Comparison with the state of the art RIS-Aided localization systems*

To benchmark the performance of the proposed SRA, we compared it with several state-of-the-art machine learning and optimization algorithms reported in [38]. These methods represent some of the most advanced strategies for RIS assisted environments, incorporating both heuristic and learning-based optimization schemes. As shown in Fig. 14, the proposed SRA algorithm achieves consistently low localization errors across all percentiles, with especially strong performance at the higher end. At the 90th percentile, the error remains as low as 19.5cm, which is better than most of the methods considered and closely matches the best performing hybrid approach (PSO-GA, 29.1cm).

One of the strengths of the SRA approach lies in its tight error distribution. The gap between the 50th and 90th percentile is less than 9cm, suggesting that the algorithm performs reliably in a wide range of cases, not just on average. This consistency indicates a strong generalization under noisy and dynamic conditions. In contrast, other optimization-based techniques often show a sharp increase in error at higher percentiles, pointing to a lack of robustness in less ideal scenarios. The stable behavior of SRA makes it a suitable candidate for applications where reliable performance is more critical than only peak accuracy.

It is worth noting that while [38] employed a high-resolution grid with 0.1 cm sampling in both x and y directions, our method operates on a coarser 25cm grid

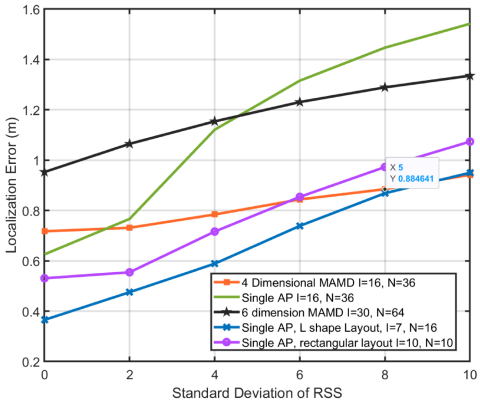

Fig. 13. SRA adaptability to different room layouts and settings.

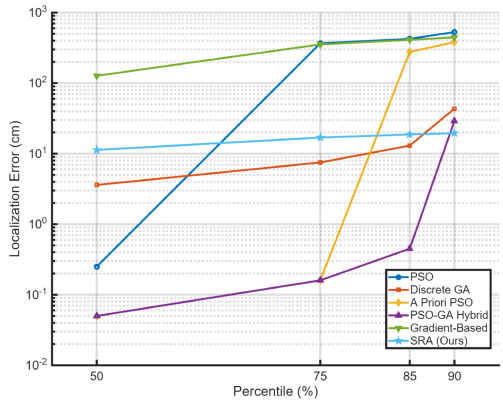

Fig. 14. localization error as a function of percentile for each method

resolution (0.5m × 0.5m cells). Despite this, the SRA achieves comparable accuracy at higher percentiles, demonstrating its robustness without requiring dense spatial sampling. The superior performance of [38] at lower percentiles is likely attributable to their finer grid, highlighting that the gain is due to resolution rather than localization strategy. Our setup, though coarser, remains competitive and more practical in real-world deployments.

We deliberately avoided further reducing the grid size, as doing so would require extremely high sampling rates to resolve time-of-arrival differences between closely spaced reference points—e.g., a 0.25m spacing demands a time resolution of 0.83ns, equivalent to a 5GS/s rate. While feasible in simulation, such requirements pose significant challenges for real-time hardware. Despite this moderate resolution, the SRA performs competitively with more complex approaches, including hybrid methods like PSO-GA, and does so without relying on extensive training data or dense spatial sampling. This highlights its practicality and efficiency for real-world RIS-assisted localization scenarios.

VII. Conclusion

This paper introduced a Static Reconfiguration Algorithm (SRA) that leverages Reconfigurable Intelligent Surfaces (RIS) to enhance indoor positioning accuracy through a Maximum Differentiated RSS (MDRSS) distribution. By eliminating dynamic reconfiguration, SRA reduces complexity while maintaining robust performance, achieving positioning errors of cm, half those of conventional methods, and sustaining sub-meter accuracy even with a single AP. The approach scales efficiently across noise levels and environments, offering a practical low-latency solution for 6G and IoT systems. Future work will explore hybrid static–dynamic schemes and lightweight machine-learning integration to adapt RIS configurations in real time while retaining SRA's efficiency and simplicity.

References

[1] M. Di Renzo *et al.*, "Smart radio environments empowered by reconfigurable intelligent surfaces: How it works, state of research, and the road ahead," *IEEE Journal on Selected Areas in Communications*, vol. 38, no. 11, pp. 2450–2525, 2020.

[2] L. Pinho, P. Gonçalves, and G. P. Dias, "Providing contextual information in smart cities with bluetooth beacons: a systematic review," in *2022 17th Iberian Conference on Information Systems and Technologies (CISTI)*, 2022, pp. 1–5.

[3] A. Cirigliano, R. Cordone, A. A. Nacci, and M. D. Santambrogio, "Toward smart building design automation: Extensible cad framework for indoor localization systems deployment," *IEEE Transactions on Computer-Aided Design of Integrated Circuits and Systems*, vol. 37, no. 1, pp. 133–145, 2018.

[4] B. Berruet, O. Baala, A. Caminada, and V. Guillet, "E-loc: Enhanced csi fingerprinting localization for massive machine-type communications in wi-fi ambient connectivity," in *2019 International Conference on Indoor Positioning and Indoor Navigation (IPIN)*, 2019, pp. 1–8.

[5] Q. Bader, S. Saleh, M. Elhabiby, and A. Noureldin, "NLoS detection for enhanced 5g mmwave-based positioning for vehicular iot applications," in *GLOBECOM 2022 - 2022 IEEE Global Communications Conference*, 2022, pp. 5643–5648.

[6] R. Moradi, M. Hutchinson, Y. Zheng, and M. Roth, "Positioning approach for train-infrastructure interaction assets health status monitoring," in *2020 European Navigation Conference (ENC)*, 2020, pp. 1–9.

[7] A. Zelenkauskaite, N. Bessis, S. Sotiriadis, and E. Asimakopoulou, "Interconnectedness of complex systems of internet of things through social network analysis for disaster management," in *2012 Fourth International Conference on Intelligent Networking and Collaborative Systems*, 2012, pp. 503–508.

[8] H. Yan, T. Peng, H. Liu, and Y. Ding, "Indoor position method of industrial robot based on wifi fingerprint position technology," in *2019 1st International Conference on Industrial Artificial Intelligence (IAI)*, 2019, pp. 1–6.

[9] A. Behravan *et al.*, "Positioning and sensing in 6g: Gaps, challenges, and opportunities," *IEEE Vehicular Technology Magazine*, vol. 18, no. 1, pp. 40–48, 2023.

[10] M. Sode *et al.*, "Reconfigurable intelligent surfaces for 6g mobile networks: An industry rd perspective," *IEEE Access*, vol. 12, pp. 163 155–163 171, 2024.

[11] E. Basar *et al.*, "Reconfigurable intelligent surfaces for 6g: Emerging hardware architectures, applications, and open challenges," *IEEE Vehicular Technology Magazine*, vol. 19, no. 3, pp. 27–47, 2024.

[12] Z. Yang, Z. Zhou, and Y. Liu, "From RSSI to CSI: Indoor localization via channel response," vol. 46, no. 2, 2013. [Online]. Available: https://doi.org/10.1145/2543581.2543592

[13] K. Wu, J. Xiao, Y. Yi, D. Chen, X. Luo, and L. M. Ni, "CSI-based indoor localization," *IEEE Transactions on Parallel and Distributed Systems*, vol. 24, no. 7, pp. 1300–1309, 2013.

[14] N. Rogel, D. Raphaeli, and O. Bialer, "Time of arrival and angle of arrival estimation algorithm in dense multipath," *IEEE Transactions on Signal Processing*, vol. 69, pp. 5907–5919, 2021.

[15] A. Makki, A. Siddig, M. Saad, J. R. Cavallaro, and C. J. Bleakley, "Indoor localization using 802.11 time differences of arrival," *IEEE Transactions on Instrumentation and Measurement*, vol. 65, no. 3, pp. 614–623, 2016.

[16] J. Sidorenko, N. Scherer-Negenborn, M. Arens, and E. Michaelsen, "Multilateration of the local position measurement," in *2016*

International Conference on Indoor Positioning and Indoor Navigation (IPIN), 2016, pp. 1–8.

[17] H. Liu, H. Darabi, P. Banerjee, and J. Liu, "Survey of wireless indoor positioning techniques and systems," *IEEE Transactions on Systems, Man, and Cybernetics, Part C (Applications and Reviews)*, vol. 37, no. 6, pp. 1067–1080, 2007.

[18] F. Zafari, A. Gkelias, and K. K. Leung, "A survey of indoor localization systems and technologies," *IEEE Communications Surveys Tutorials*, vol. 21, no. 3, pp. 2568–2599, 2019.

[19] E. Basar *et al.*, "Wireless communications through reconfigurable intelligent surfaces," *IEEE Access*, vol. 7, pp. 116 753–116 773, 2019.

[20] T. Ma *et al.*, "Reconfigurable intelligent surface-assisted localization: Technologies, challenges, and the road ahead," *IEEE Open Journal of the Communications Society*, vol. 4, pp. 1430–1451, 2023.

[21] T. Ma, Y. Xiao, X. Lei, W. Xiong, and M. Xiao, "Distributed reconfigurable intelligent surfaces assisted indoor positioning," *IEEE Transactions on Wireless Communications*, vol. 22, no. 1, pp. 47–58, 2023.

[22] C. L. Nguyen, O. Georgiou, G. Gradoni, and M. Di Renzo, "Wireless fingerprinting localization in smart environments using reconfigurable intelligent surfaces," *IEEE Access*, vol. 9, pp. 135 526–135 541, 2021.

[23] T. Ma, Y. Xiao, X. Lei, W. Xiong, and Y. Ding, "Indoor localization with reconfigurable intelligent surface," *IEEE Communications Letters*, vol. 25, no. 1, pp. 161–165, 2021.

[24] H. Zhang, H. Zhang, B. Di, K. Bian, Z. Han, and L. Song, "Towards ubiquitous positioning by leveraging reconfigurable intelligent surface," *IEEE Communications Letters*, vol. 25, no. 1, pp. 284–288, 2021.

[25] F. Zafari, A. Gkelias, and K. K. Leung, "A survey of indoor localization systems and technologies," *IEEE Communications Surveys Tutorials*, vol. 21, no. 3, pp. 2568–2599, 2019.

[26] N. Afzali, M. J. Omidi, K. Navaie, and N. S. Moayedian, "Low complexity multi-user indoor localization using reconfigurable intelligent surface," in *2022 30th International Conference on Electrical Engineering (ICEE)*, 2022, pp. 731–736.

[27] S. Hassouna, M. A. Jamshed, M. Ur-Rehman, M. A. Imran, and Q. H. Abbasi, "Ris-assisted near-field localization using practical phase shift model," *Scientific Reports*, vol. 14, no. 1, pp. 1–10, 2024.

[28] R. A. Aguiar, N. Paulino, and L. M. Pessoa, "A deep learning approach in ris-based indoor localization," in *2024 Joint European Conference on Networks and Communications 6G Summit (EuCNC/6G Summit)*, 2024, pp. 523–528.

[29] Q. Pu *et al.*, "Ris-aided indoor positioning system based on passive reflective elements optimization," *IEEE Transactions on Vehicular Technology*, vol. 73, no. 11, pp. 17 095–17 105, 2024.

[30] A. Saleh and R. Valenzuela, "A statistical model for indoor multipath propagation," *IEEE Journal on Selected Areas in Communications*, vol. 5, no. 2, pp. 128–137, 1987.

[31] A. A. Hussein, T. A. Rahman, and C. Y. Leow, "Performance evaluation of localization accuracy for a log-normal shadow fading wireless sensor network under physical barrier attacks," *Sensors*, vol. 15, no. 12, pp. 30 545–30 570, 2015.

[32] P. Bahl and V. Padmanabhan, "Radar: an in-building rf-based user location and tracking system," in *Proceedings IEEE INFOCOM 2000. Conference on Computer Communications. Nineteenth Annual Joint Conference of the IEEE Computer and Communications Societies (Cat. No.00CH37064)*, vol. 2, 2000, pp. 775–784 vol.2.

[33] M. Youssef and A. Agrawala, "The Horus WLAN location determination system," *Wireless Networks*, vol. 14, no. 3, pp. 357–374, 2005.

[34] F. Saggese *et al.*, "Control aspects for using ris in latency-constrained mobile edge computing," in *2023 57th Asilomar Conference on Signals, Systems, and Computers*, 2023, pp. 174–181.

[35] H. Zhang, H. Zhang, B. Di, K. Bian, Z. Han, and L. Song, "Metalocalization: Reconfigurable intelligent surface aided multi-user wireless indoor localization," *IEEE Transactions on Wireless Communications*, vol. 20, no. 12, pp. 7743–7757, 2021.

[36] Z. Zhang *et al.*, "Multiple rss fingerprint based indoor localization in ris-assisted 5g wireless communication system," in *The International Archives of the Photogrammetry, Remote Sensing and Spatial Information Sciences*, vol. XLVI-3/W1-2022, 2022, pp. 287–294, proc. 7th Intl. Conf. on Ubiquitous Positioning, Indoor Navigation and Location-Based Services (UPINLBS 2022), Wuhan, China.

[37] S. T. Shah *et al.*, "Coded environments: data-driven indoor localisation with reconfigurable intelligent surfaces," *Communications Engineering*, vol. 3, p. 66, 2024.

[38] R. A. Aguiar, N. Paulino, and L. M. Pessoa, "Enhancing nlos ris-aided localization with optimization and machine learning," in *2023 IEEE Globecom Workshops (GC Wkshps)*, 2023, pp. 1898–1903.